



# Synthesis and properties of graphene and graphene/carbon nanotube-reinforced soft magnetic FeCo alloy composites by spark plasma sintering

Amar J. Albaaji<sup>1,\*</sup>, Elinor G. Castle<sup>2,3</sup>, Mike J. Reece<sup>2,3</sup>, Jeremy P. Hall<sup>1</sup>, and Sam L. Evans<sup>4</sup>

<sup>1</sup>Cardiff School of Engineering, Wolfson Centre for Magnetics, Cardiff University, Cardiff, UK

<sup>2</sup>School of Engineering and Materials Science, Queen Mary University of London, London, UK

<sup>3</sup>Nanoforce Technology Ltd., London, UK

<sup>4</sup>Cardiff School of Engineering, Institute of Mechanical and Manufacturing Engineering, Cardiff University, Cardiff, UK

Received: 27 February 2016

Accepted: 4 May 2016

Published online:

11 May 2016

© Springer Science+Business Media New York 2016

## ABSTRACT

The effect of the addition of graphene nanoplatelets (GNP) and graphene nanoplatelet/carbon nanotube (GNT) mixtures on the mechanical and magnetic properties of spark plasma sintered soft magnetic FeCo alloys was studied. Three different volume fractions (0.5, 1 and 2 vol%) of GNPs and GNTs were investigated. Ball milling was used to disperse the GNPs in monolithic FeCo powder, while magnetic stirring and ultrasonic agitation were used to prepare hybrid GNT prior to ball milling. The highest saturation induction ( $B_{\text{sat}}$ ) of 2.39 T was observed in the 1 vol% GNP composite. An increase in the volume fraction of the ordered nanocrystalline structure was found to reduce the coercivity ( $H_c$ ) of the composites. The addition of CNTs to the GNP composite prevented grain growth, leading to grain refinement. An 18 % increase in hardness was observed in the 1 vol% GNP composite as compared to the as-received FeCo alloy. A reduction in tensile strength was observed in all of the composite materials, except for the 0.5 vol% GNT composite, for which a value of 643 MPa was observed. Raman spectroscopy indicated a reduction in the defect density of the GNPs after adding CNTs.

## Introduction

Graphene is a material composed of  $sp^2$  carbon atoms arranged in a two-dimensional honeycomb structure and is the strongest material ever recorded [1].

Graphene sheets stack on top of one another, leading to weak van der Waals forces in the c-axis with an approximate separation distance of 3.4 Å. Graphene nanoplatelets (GNPs) typically consist of a ~100-nm-thick stack of graphene sheets [2, 3]. Due to its unique

Address correspondence to E-mail: amar.jabar@yahoo.com

electrical, thermal and mechanical properties [4, 5], graphene has the potential to significantly improve the properties of materials through its addition as a second phase.

Intermetallic compounds generally exhibit a very low level of ductility at room temperature. Due to the formation of the ordered B2 state, near equiatomic FeCo alloys exhibit very good magnetic properties, yet they are extremely brittle at room temperature. Modern power generation systems demand new materials with both good magnetic and mechanical properties. The magnetic properties of FeCo alloys satisfy this requirement; however, the mechanical properties of FeCo alloy must be improved in order to meet this need. An improvement in the ductility of the FeCo alloy has been achieved through grain refinement, reducing the degree of ordering and addition of the alloying element vanadium [6]. Kawahara [7] tested the effect of combined cold working and heat treatment plus the addition of different alloying elements on the magnetic and mechanical properties of FeCo alloys. He reported that the magnetic and mechanical properties are effectively improved by the addition of C, V, Cr, Ni, Nb, Mo, Ta and W. A model for the improvement of ductility in FeCo alloys has been suggested by adding carbon in [8]. Yu et al. [9] electrodeposited FeCo alloys onto W fibres. An improvement in mechanical properties was achieved; however, non-soft magnetic behaviour in the as-deposited composite was observed due to the stresses introduced by the fabrication process. Powder metallurgy followed by ball milling is considered to be the best route to manufacture extremely brittle FeCo alloy components, since there is more flexibility in the final dimensions and shape and a high mechanical strength can be achieved with little effect on the magnetic properties [10]. Almost all properties, including strength, ductility and magnetic performance, are improved with increasing density in powder metallurgy products [11].

The spark plasma sintering (SPS) process has been used extensively in the last decade to densify a wide variety of powdered materials. The application of high pressure and pulsed DC current to the electrically conductive dies leads to rapid heating and sintering. As such, the technique makes it possible to achieve high densities, close to theoretical density, without prior compaction or binder addition. The rapid nature of the technique enables

the characteristics of the starting powder to be transferred to the final sintered part, such as a fine-grained size, metastable phase, or composition or inclusion of volatile elements. The application of a current during processing has been shown to ‘clean’ the powder particles of surface oxides [12, 13]. Many studies have employed SPS to sintering carbon nanotube (CNT) composites and nanopowders with the aim of restricting grain growth [2, 14]. Mani et al. obtained 99 % theoretical density and a saturation induction ( $B_{\text{sat}}$ ) of 2.33 T in Fe-50 % Co alloy prepared by SPS at 900 °C for 2–5 min under a pressure of 80 MPa [15]. Recently, a Ni-P electroless-coated CNT-reinforced Fe-50 Co composite was fabricated by ball milling and SPS processing; an improvement in ductility and strength was observed at the expense of the magnetic properties [16]. The phase transformation of metal magnetic alloys during processing effects the processing parameters of the SPS furnace, making it is possible to calibrate temperature [17].

While extensive research has been published on polymer–graphene composites [1] and to a lesser extent on ceramic–graphene composites [18], to the best of our knowledge, there are very limited publications on metal graphene composites, especially FeCo alloys. Issues involving the formation a stable dispersion of GNPs are rather complicated as compared to CNTs since GNPs tend to agglomerate and restack on one another during dispersion and drying.

Kim et al. [19] used graphene oxide as a dispersion agent for both multi-walled and single-walled carbon nanotubes in water. The authors demonstrate that graphene oxide is able to strongly interact with the surface of CNTs throughout  $\pi$ – $\pi$  attractions due to many  $\pi$ -conjugated on the surface of graphene oxide. Wimalasiri et al. [20] have used single-walled carbon nanotubes (SWCNTs) to prevent restacking between graphene sheets when they fabricated electrodes from carbon nanotube and graphene composite. Increasing the space between graphene using CNTs improves the transport of electrolyte ions within the electrode. This strategy has been previously tested in ceramic [21, 22], polymer [23] and light weight metal alloy [24]-based systems. Excellent mechanical properties due to improved dispersions were achieved. So far, there has been no systematic study into the use of CNTs to improve the dispersion of GNPs in soft magnetic FeCo alloys.

This article outlines the results from a study into the effects of GNP and CNT additions on the structural, magnetic and mechanical properties of Fe–Co composites fabricated by ball milling and SPS.

## Materials and methods

### Starting materials

Gas-atomised FeCo alloy powder was supplied by Sandvik Osprey Powder Group. The mean size of powder, measured by Malvern Mastersizer 3000 with laser scattering, is 23.4  $\mu\text{m}$ . Multi-walled carbon nanotubes (MWCNT) and GNP were provided from Haydale Ltd. They are functionalized by plasma treatment to incorporate covalently bonded oxide group on their surfaces.

### Powder mixing

GNP was dispersed in FeCo powder using Spectro-mill ball pestle impact grinder in air atmosphere (Chemplex Industries Inc., Model 1100) with steel ball pestles with a ball to powder ratio (BPR) of  $\sim 1:1$  for 1 h. Three different volume fractions (0.5, 1 and 2 vol%) of GNP were dispersed in 20 g of FeCo powders. The mixture of CNT and GNP referred to as GNT was also used as reinforcement for soft magnetic FeCo alloy at same volume fraction. The mixing ratio of CNT:GNP was 1:10. The theoretical densities used to calculate of the volume fractions using a rule of mixture are 1.4, 2.2 and 8.174  $\text{g cm}^{-3}$  for CNT, GNP and FeCo powder, respectively. GNT was magnetically stirred in 100 ml of ethanol for 0.5 h, followed by ultrasonication for 0.5 h. Twenty grams of FeCo powder was mixed with GNT to form composite slurry. The composite mixture was tip sonicated for 1 h in 150 ml ethanol. Drying was performed by heating at 80  $^{\circ}\text{C}$  on hot plate overnight. After drying, the powder was ball milled using the same conditions described for the GNP dispersions.

### SPS fabrication

Twenty grams of FeCo alloy powders and composite powder mixtures were consolidated in a graphite die lined with graphite foil using a SPS furnace (HPD 25/1 FCT, Germany). All of the samples were heated to the sintering temperature at a constant rate of

50  $^{\circ}\text{C min}^{-1}$  under a vacuum of 1.5 Pa. The initial 7 MPa pressure was applied to 400  $^{\circ}\text{C}$ ; followed by an increase to 80 MPa pressure and simultaneous heating to 900  $^{\circ}\text{C}$  for a 3-min soak at this temperature [15]. After rapid cooling in contact with the water-cooled pistons of the SPS furnace, the samples were manually extracted from the die using a hydraulic press.

### Characterisation

In order to measure the density of the sintered materials, the graphite layer was removed from surface of sintered materials by grinding with Emery paper. The density was measured using Archimedes' immersion method in water. To evaluate the structure of raw nanomaterials, a high-resolution transmission electron microscope (TEM) (JEM-2100LaB6) was used to evaluate the as-received GNPs and CNTs. For optical microscopy analysis, cross-sections of the sintered materials were ground and polished with different grade abrasive discs followed by etching using 10 % Nital for 30 s. Scanning electron microscopy (SEM) (Oxford instruments) was used to analyse the fracture surfaces of the tensile samples. The crystallographic phases and ordering state present in the as-received and composite materials were examined using X-ray diffraction (XRD) (Philips PW 3830 automated powder diffraction) supplied with a Co target X-ray tube. The scans were performed between 10 and 110  $^{\circ}2\theta$  at a scan speed of  $8 \times 10^{-3}$   $^{\circ}2\theta \text{ sec}^{-1}$  at operation conditions of 35 kV and 40 mA. A slow scan was performed in the expected  $^{\circ}2\theta$  range of the ordered phase at a scan speed of  $25 \times 10^{-5}$   $^{\circ}2\theta \text{ sec}^{-1}$  and operating conditions of 42 kV and 40 mA.

Raman spectroscopy was performed on the GNP and CNT powders and on tensile samples of composites of different volume fractions (using Renishaw inVia Raman microscope). The excitation wavelength was maintained at 514 nm for all samples with a power of 25 mW and spot size of 5  $\mu\text{m}$ . The Raman spectra scans between 1000 and 3200  $\text{cm}^{-1}$  were obtained after 15 accumulations.

### Mechanical and magnetic properties

Tensile tests were performed on three samples cut from the 30 mm diameter monolithic FeCo alloy and composites discs by electron-discharge machining

(EDM). The cut samples were ground with silicon carbide to remove any crack initiation sites produced by cutting. Tensile properties were evaluated using a Shimadzu testing machine with a cross head speed of  $2 \text{ mm min}^{-1}$ . The tensile sample dimensions in mm were  $11 \times 3 \times 1.25$  [25]. Hardness measurements for both the matrix alloy and composite were performed at five different locations using a Vickers hardness tester using 30 g load for 4 s. In order to evaluate the magnetic properties, samples with a rectangular cross section  $24 \times 5 \text{ mm}$  were cut from the 30 mm diameter sintered discs using an EDM cutting machine. Samples were ground using Emery paper to remove the scratches produced during cutting. An automatic universal measurement system was used to evaluate the quasi DC magnetic response for samples by changing the magnetic field up to  $25 \text{ kA m}^{-1}$  [26].

## Results and discussion

### TEM analysis of nanopowder

The GNPs and carbon nanotube morphologies are shown in Fig. 1. A wrinkled morphology is observed for the GNPs, which may produce porosity in the composites. A variety of sizes were observed, and very small sheets were observed to be stacked on larger sheets. The thickness of the GNP sheets ranges from  $\sim 4$  to 42 nm. The width of the sheets ranges from  $\sim 27$  to 223 nm, while the length varies from  $\sim 85$  to 487 nm. Most of CNTs are tangled together, which impedes their dispersion. The measured dimensions of the CNTs exhibit a mean outer diameter of around 10.45 nm, while the inner diameter is around  $\sim 4$  nm (corresponding, to  $\sim 10$  concentric shells of carbon sheets).

### Optical microstructure

The optical micrographs of the monolithic FeCo alloy and composite materials are shown in Fig. 2. The as-received monolithic FeCo alloy consists of grains of uniform size, as shown in Fig. 2a. The sintered samples prepared with powders that had been ball milled contained elongated grains, as shown in Fig. 2b. The microstructure of the GNP composites was inhomogeneous (Fig. 2c) with excessively growth grains surrounded by small grains. Adding a small amount of CNTs (1:10) significantly changes the

microstructure. The homogenous microstructure observed may result from the uniform dispersion of the nanophases and the prevention of their stacking of the nanophases. Figure 2d shows the refined microstructure, which is occurred due to the addition CNTs to GNPs as compared to the GNP composite (Fig. 2c). An increase in the volume fraction of reinforcement leads to the introduction of agglomerates, which results in increased porosity. Impurity elements such as (O, N and  $\text{H}_2$ ) may segregate at grain boundaries, and grain boundaries were investigated using EDX spectra. The spectra were taken from the grain boundaries of sintered 1 vol% GNP and FeCo alloy did not show any difference in chemical composition between materials.

### Densification of sintered FeCo composites

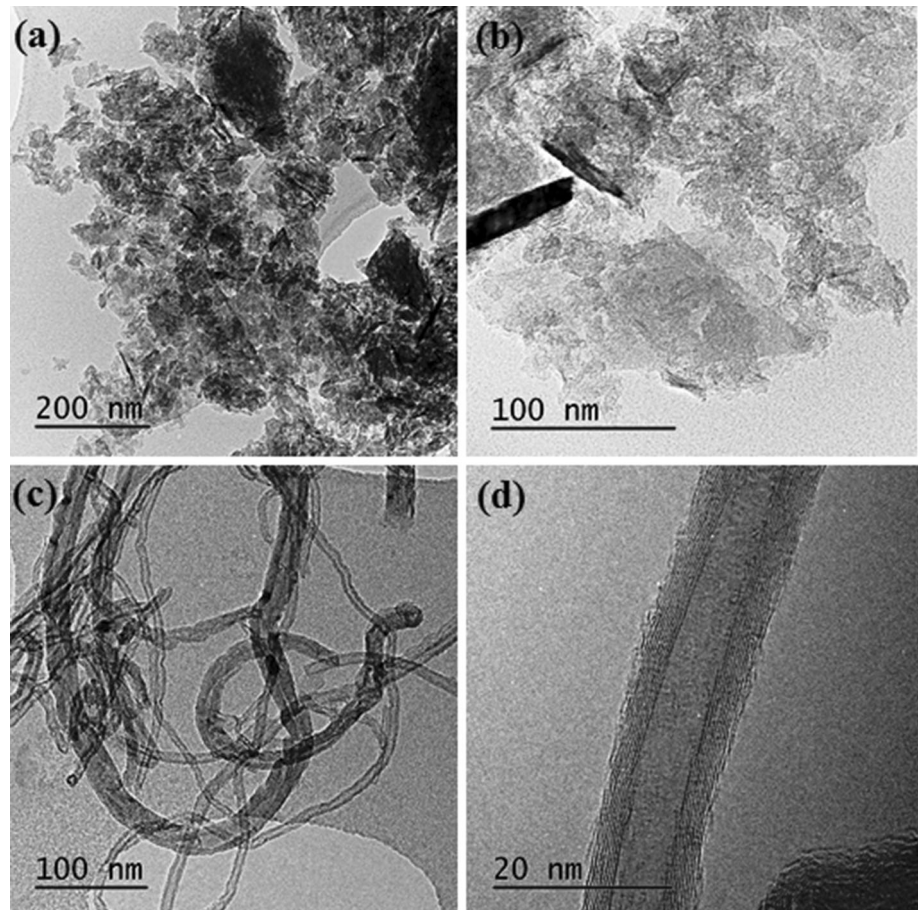
The relative density of the spark plasma sintered FeCo-GNP and FeCo-GNT compacts are shown in Fig. 3. Almost full densification was achieved for the as-received FeCo compact, with a relative density higher than 99 %. In comparison, the final density of the FeCo alloy after 1-h ball milling was reduced to 98 %. The addition of reinforcements increased the final density in comparison to the ball milled FeCo alloy, yet it decreased overall with increasing volume fraction of reinforcement. The density of the GNT composites was lower as compared to the GNP composites, which might be attributed to the presence of carbon nanotubes in the GNT composites. The 2D morphology of the GNPs leads to a higher surface area as compared to the 1D carbon nanotubes. An increase in the contact area between the GNPs and the matrix alloy leads to a higher density, while CNTs inserted between the GNPs may introduce porosity between the sheets and reduce the density.

### Analysis X-ray diffraction results of raw materials and FeCo composites

XRD patterns of the sintered FeCo alloy and its composites are presented in Fig. 4. In spite of the slow X-ray scan rate used for all of the FeCo alloy composites, the distinctive  $2\theta = 26.5^\circ$  peak of the GNPs was not observed due to its relatively low volume fractions, which are beyond the sensitivity of the XRD technique. To clarify any shift in peaks position, the figure was enlarged, as shown in the inset (Fig. 4). The fundamental peaks were shifted to



**Figure 1** Transmission electron microscope (TEM) of a, b GNP and c, d CNT.



lower angles in the composite materials as compared to the as-received FeCo alloy. This is due to the stresses introduced during ball milling. A broadening of the XRD peaks was also observed in the composite materials, due to microstructure refinement following ball milling. The volume fraction of the ordered state has an effect on both the magnetic and mechanical properties of FeCo alloys. A very slow scan rate and high intensity XRD ( $\text{Co } K\alpha$ ) was employed in order to investigate the (100) super lattice line reflection of the sintered FeCo alloy, 1-h ball milled FeCo alloy, GNT and GNP composites as shown in Fig. 5. The long-range ordering fraction in FeCo alloy has been shown to reduce following ball mill [27]. With 1 vol% GNP dispersion in the FeCo alloy, an increased volume fraction of ordering was observed. However, the introduction of 2 vol% GNP did not make any significant difference to the degree of ordering and crystallite size. The intensity of the super lattice reflection was found to be higher in the GNP composites as compared to the GNT composites, indicating a greater volume fraction of ordering in the

GNP composite. This is confirmed by the shift of the peak to lower angles in the GNP composites due to the strains induced by the more significant ordering reaction as compared to the GNT composites. Clegg and Buckley [28] reported that the change in lattice parameter between the disordered and ordered phases is about 0.2 %, varying from 0.28550 to 0.28570 nm. The anti-phase domain sizes were estimated from the super lattice line in Fig. 5 using the Scherrer equation. A significant reduction in the anti-phase domain sizes was observed in the 1 vol% GNT composite, which reflects the role of carbon nanotubes in refining the crystallite structure or due to improved dispersion, while GNP additions did not influence the nanostructure.

### Magnetic properties

A summary of the magnetic induction ( $B_{\text{sat.}}$ ), coercivity ( $H_c$ ) and remanence ( $B_r$ ) of the materials is shown in Fig. 6. An increase in saturation induction and reduction in coercivity is observed in the GNP

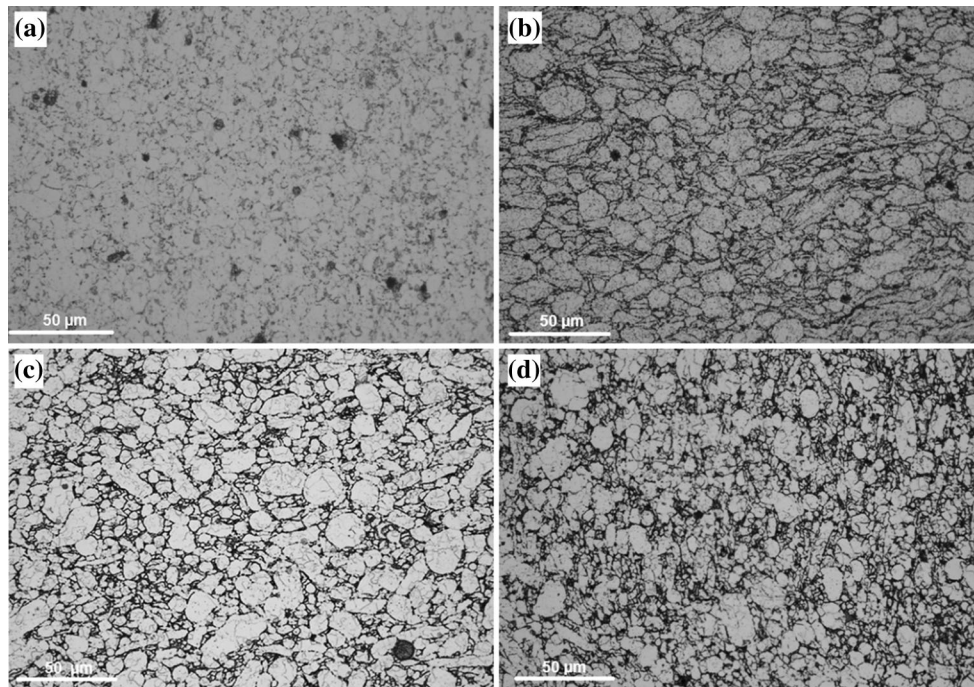


**Figure 2** Optical microstructure of **a** as-received FeCo alloy, **b** 1-h ball milling FeCo compact, **c** 2 vol% GNP composite, **d** 2 vol% GNT composite.

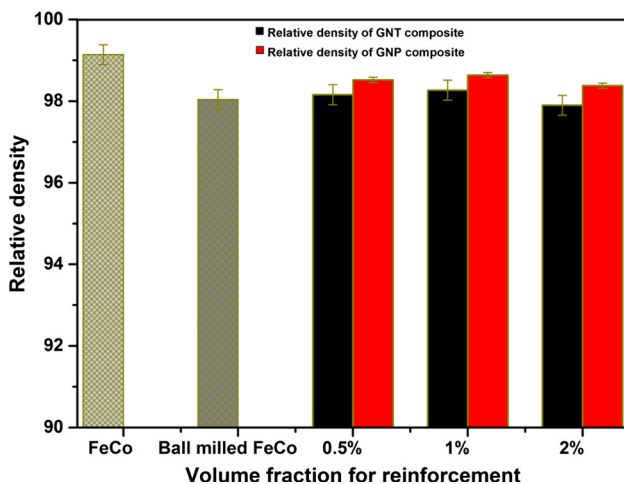


**Figure 3** Variation of relative density of SPS sintered composite materials against volume fraction of GNP and GNT (vol%) as compared to the monolithic FeCo alloy.

composites compared to as-received FeCo alloy, for reinforcement additions up to 1 vol%. In general, a higher remanence is observed in the GNT composite as compared to the GNP composites (Fig. 6, inset). In order to separate the effects of ball milling from the effect of reinforcement on the magnetic properties, the 1-h ball milled FeCo compact was also investigated. The saturation induction of 1-h ball milled

FeCo compact was reduced from 2.30 to 2.23 T, while exhibiting a decline in coercivity from 836 to 763 A m<sup>-1</sup>.

It was shown in the previous section that the density after ball milling under air atmosphere dropped, which can account for the reduced in saturation induction due to oxide formation [27]. The 1 vol% of GNPs composite exhibited a higher saturation induction value of 2.39 T than the 1-h ball mill FeCo alloy (2.23 T) due to the increase in density produced by the addition GNPs to the ball milled FeCo alloy as confirmed in Fig. 3. However, with addition of 1 vol% of GNTs, the saturation induction dropped to 2.12 T. The increased space between GNPs due to inserting CNTs leads to drop in density due to formation porosity between sheets (Fig. 3). Further, the increased saturation in GNP composite can also be explained by the ferromagnetic behaviour of graphene and improved electrical conductivity of this composite [29, 30], which could affect the densification processes during SPS and subsequent magnetic properties. The 2D form of the GNPs exhibits open edges, in contrast to the inserted CNTs which have closed  $\pi$ -electron systems. The non-bonding state also creates nanomagnetic properties at edges [31]. However, the inserted CNTs will



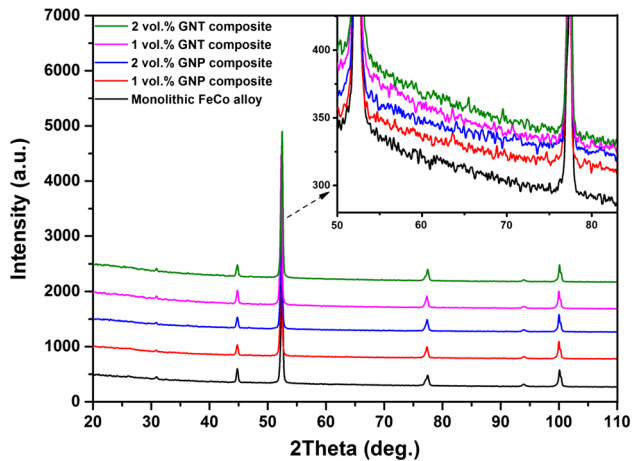


**Figure 4** XRD patterns for FeCo as-received 1 vol% GNP composite, 2 vol% GNP composite, 1 vol% GNT and 2 vol% GNT composite.

influence magnetic properties primarily due to the introduction of porosity and due to the presence of any residual metallic catalysts on their surface.

The coercivity is sensitive to the change in microstructure. The plastic deformation has significant effect on coercivity, like the increased dislocation density from deformation stresses which may change the anisotropy constant  $K_1$ , leading to effect on coercivity value [32]. The ball milling was used here with all samples for limited time of 1 h and low BPR of  $\sim(1:1)$  as a result of that the effect of ball milling stresses was not significant on the coercivity or stresses were released during the cooling in SPS furnace. The coercivity after ball milling under air atmosphere dropped, which may have been caused by the formation of nanocrystalline structure. The slow scan rates XRD (CoK $\alpha$ ) patterns (Fig. 5) revealed a (100) super lattice reflection with crystallite dimensions reduced to nanoscale. It has been shown [33, 34] that at this scale the trend in coercivity would follow that of the average magneto-crystalline anisotropy when the crystallite size becomes less than the ferromagnetic exchange length, leading to a drop in coercivity. The composites with GNT displayed a higher coercivity than the GNP composites, which is due to the more refined grain size (Fig. 2d) of GNT composite as a result of better dispersion. The restacking of GNPs increased at higher volume fraction composites, leading to an increase of the particle size of the GNPs to micron size, which decreases the effectiveness of GNPs to reduce grain growth.

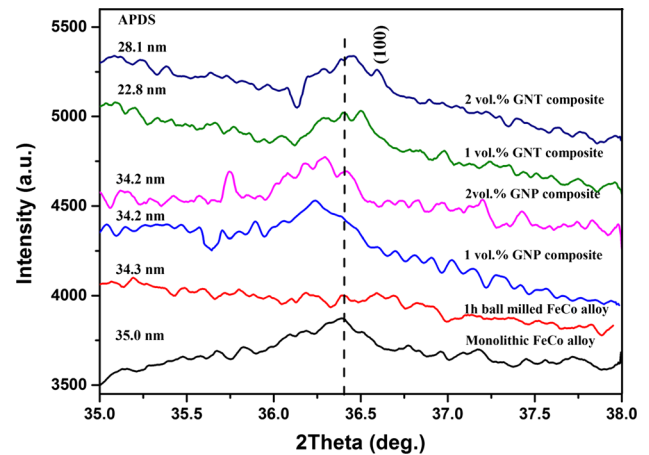


**Figure 5** Slow scan XRD patterns show (100) super lattice line reflection with anti-phase domain size (APDS) of monolithic FeCo alloy, 1-h ball milled FeCo alloy and displayed composites.

## Mechanical properties

The tensile strength, the mechanical hardness and failure strain of the as-received monolithic FeCo alloy (represented as 0 vol% reinforcement), and the composites with different volume fraction of GNPs and GNTs are summarised in Figs. 7 and 8, respectively. The 1-h ball milled FeCo compact was also examined and compared to alloy prepared with unmilled powder exhibited a decrease in ultimate tensile strength from  $673 \pm 17.43$  to  $643 \pm 40$  MPa; failure strain was also dropped from  $2.9 \pm 0.70$  to 2.4 %, while the hardness increased from  $326.5 \pm 18$  to  $355.7 \pm 5$  VHN.

Hard oxides formed during ball milling lead to an increase in hardness, yet they hindered densification process and hence lowered the tensile strength and failure strain. The addition of GNPs to the FeCo alloy led to a decrease in tensile strength. This was possibly due to the restacking of GNP sheets as shown in Fig. 10c, which cause easily slip in GNPs with respect to one another and separate under stresses. Strength arising from nano-reinforcement mechanisms will deteriorate once the GNPs become agglomerated into micro-sized clusters, reducing the tensile strength by acting as stress concentrators. An improvement in tensile strength was subsequently observed in the hybrid GNT composite, where the addition of CNTs prevents agglomeration of the GNPs. A marked increase in hardness to  $385.3 \pm 35$  VHN was observed in the FeCo-1 vol% GNP composite, as shown in Fig. 7. This represents an 18 % increase in hardness in

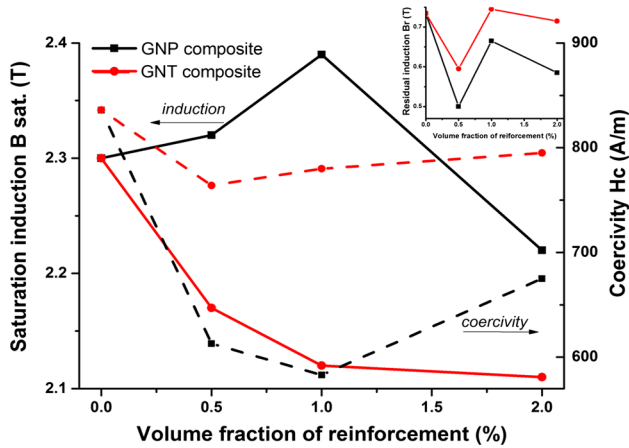


**Figure 6** Effect of volume fraction of GNP and GNT on saturation induction (solid lines), coercivity (dashed lines) and remanence (inset) of (Fe50Co) composites fabricated by spark plasma sintering.

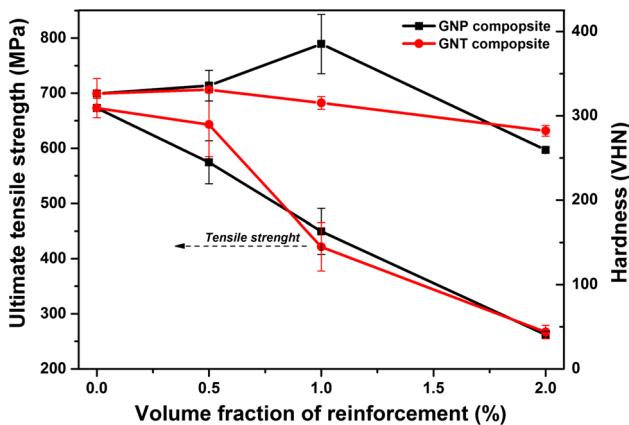


**Figure 7** Effect of volume fraction of GNP and GNT on tensile strength and hardness of Fe50Co composites fabricated by spark plasma sintering.

comparison to the as-received FeCo alloy. The highest density value among the composite materials was achieved for the 1 vol% GNP composite, leading to increase in hardness. The hardness decreased for the 2 vol% GNP composite, because of the decrease in density produced by agglomeration of GNPs.

Figure 8 shows failure strains with volume fraction of reinforcement, and the composite materials exhibit decrease in failure strain especially at higher loading as compared to the as-received FeCo alloy, confirming increased brittleness in FeCo alloy from agglomeration.

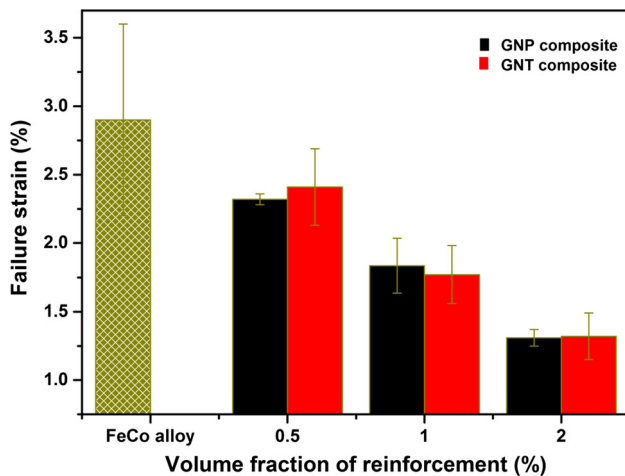
Figure 9 shows a comparison between the fracture surfaces of monolithic FeCo alloy, 1 vol% GNP

composite and 1 vol% GNT composite. Mixed mode of intergranular and transgranular fracture predominate in all of the sintered materials, indicating that the inherent weakness of grain boundaries cannot be avoided here by the nanophase additions. Evidence of toughening mechanisms, such as crack deflection and platelet pull-out, is observed in Fig. 10a, c. A large GNP can be seen to warp around a grain. It is expected that the flexibility of GNPs allows them to bend around and become embedded between the grains during sintering. The large surface area of GNPs increases the contact area with the matrix, leading to an increased interfacial force, requiring more energy to pull-out the GNP sheets as compared to the CNTs. However, overlapping between GNPs decreases the interface bonding efficiency. It is observed that thin GNP sheets are effective at inhabiting crack propagation as compared to thick overlapped GNP sheets, which are easily sheared and form pores, degrading the mechanical and physical properties. The CNTs are embedded between the GNPs as observed in Fig. 10d; pull-out of the CNTs occurred during fracture. The high aspect ratio of the CNTs allows them to bridge the fracture surface, as shown in Fig. 10b.

### Raman spectroscopy

Graphene is routinely characterised using Raman spectroscopy. In a typical Raman spectrum of single-layer graphene, the main peaks are seen at  $1583\text{ cm}^{-1}$  (commonly referred to as G), D peak at  $1350\text{ cm}^{-1}$  and the shoulder D' at around  $1620\text{ cm}^{-1}$ . In addition to this: the overtone peak, 2D or G', appears at  $2680\text{ cm}^{-1}$ ; the D + G peak appears at around  $2950\text{ cm}^{-1}$ ; the 2D' peak appears at  $3245\text{ cm}^{-1}$ ; and finally the 2D + G peak occurs at  $4290\text{ cm}^{-1}$  [35]. The ratio ( $R = I_D/I_G$ ) is typically used to measure the disorder and defect density in graphene, while the strain in graphite can be observed as a shifting and splitting of the Raman modes [36]. Raman spectra of the as-received GNP, FeCo alloy and the FeCo alloy-GNP and GNT composites are shown in Fig. 11. The FeCo alloy does not produce any Raman signals. The structure of GNP was retained after all of the fabrication processes as evidenced from the shape of the single-peak shape of the 2D band in the Raman spectrum, indicating the presence of the graphene morphology as opposed to the graphite morphology, which would give rise to a split peak [37].

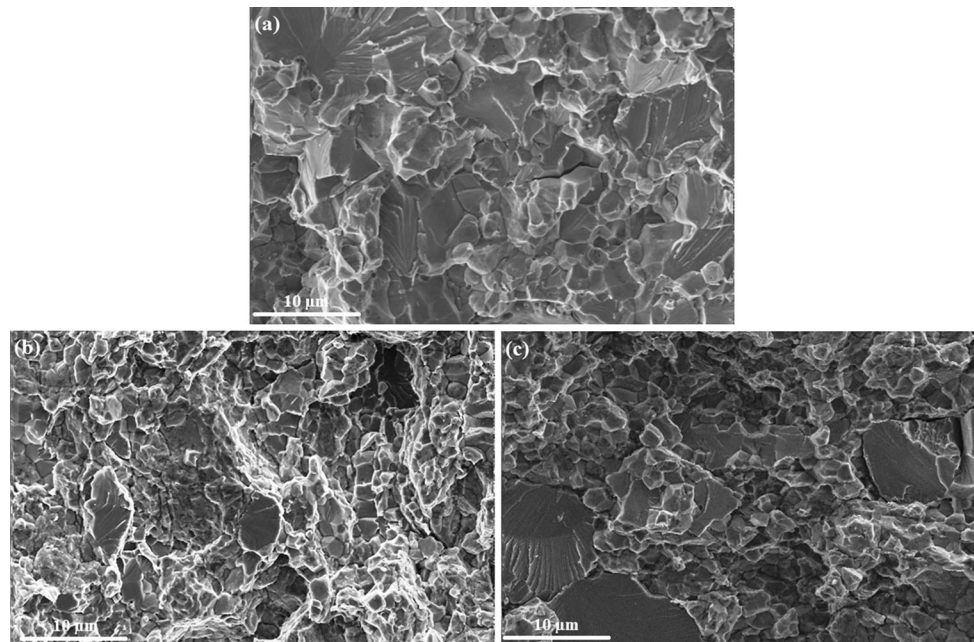




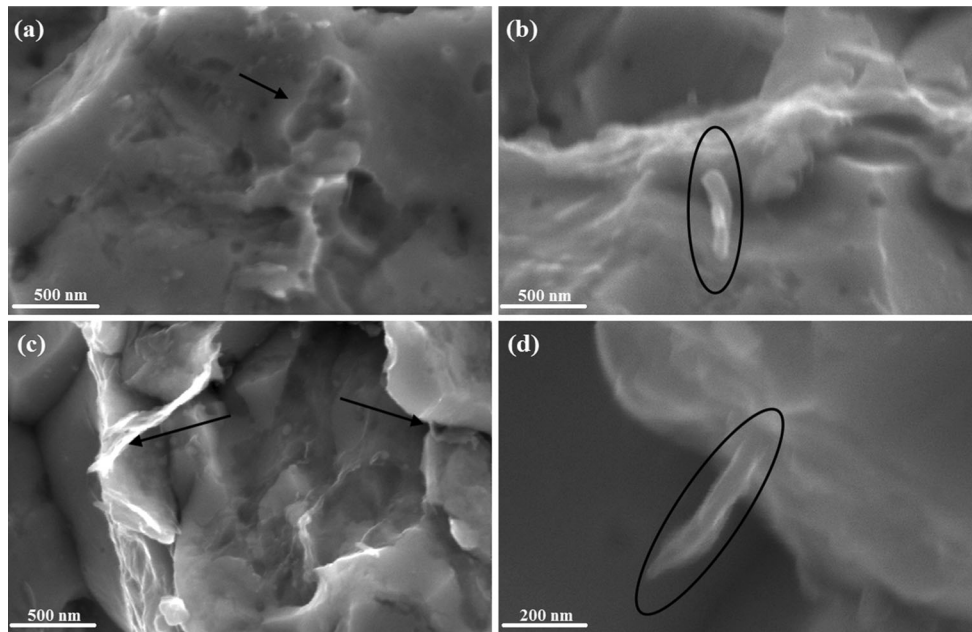
**Figure 8** Effect of volume fraction of GNP and GNT on failure strain of Fe50Co composites fabricated by spark plasma sintering.

Table 1 lists the peak intensity ratio ( $R = I_D/I_G$ ), the position of the G and 2D peak positions. The GNPs were observed to be of higher quality than the CNTs, as evidenced from the lower  $R$  ratio of the GNPs (1.00) compared to CNTs (1.11). An increase in  $R$  ratio was observed for all of the composites. This was particularly notable for the GNP composites as compared to the as-received GNPs. This may have resulted from an

interfacial reaction of the matrix with the side wall of the GNPs, or could have induced by ball milling. However, this ratio decreased in the GNT composites as compared to the GNP composites, suggesting that the addition of CNT to GNP in ethanol may help to maintain the structure of the GNP. High quality for vacuum during sintering process is crucial to preservation carbon nanostructure in sintered composites materials [38]. The oxidation for reinforcement was reduced due to using a good vacuum (1.5 Pa), which also aids in releasing oxides effectively from GNP when CNTs were inserted between sheets, helping improve the quality of carbon nanostructure. Strains are induced in the GNPs by the fabrication processes and by mechanical testing of the composite material. Such strains will lead to alterations in the interatomic distance of the graphene. The G band peak position is very sensitive to strain in the graphene structure. Hence the shift in wave number will change according to alteration in the vibration frequency of the G band due to strain [36]. Up shifting was observed in the peak position of the G band ( $\omega_G$ ) peak for the composites in comparison to the as-received GNP. A shift of between 8.6 and 22.8  $\text{cm}^{-1}$  is observed in the GNP composites as compared to the as-received GNP; a 10.6–13.6  $\text{cm}^{-1}$  shift is observed for the GNT



**Figure 9** Fractographic images of **a** as-received FeCo alloy, **b** 1 vol% GNP composites and **c** 1 vol% GNT composites fabricated by spark plasma sintering.



**Figure 10** High magnification of fractographic images **a, c** 0.5 and 1 vol% GNP composites, respectively; **b, d** 0.5 and 1 vol% GNT composites, respectively. The *arrows* show pull-out of GNP

**(a)**, thin and overlapped GNP**(c)**. Ellipses exhibit CNTs bridging **(b)** and pull-out from GNPs **(d)**.

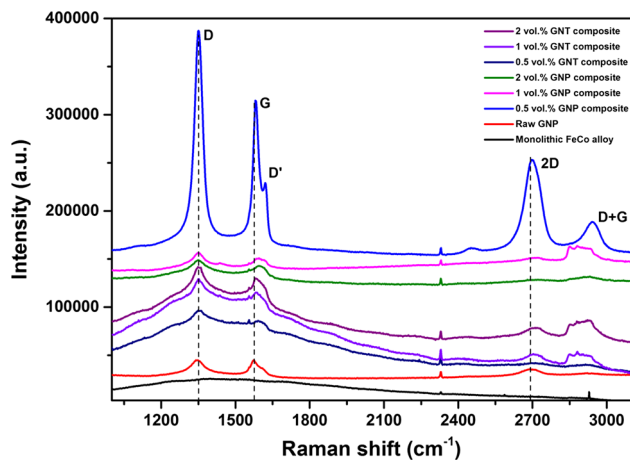


**Figure 11** Raman spectra of GNP, GNT composites and as-received graphene.

composites. This indicates that significant strains have been induced in the GNPs in the aforementioned composites. Up shifting is also observed in the 2D peak. Since the 2D band peak is very sensitive to the number of layers in graphene, a change in position, width and shape could occur in the 2D peak with an increasing number of layers [37]. The shifting was reduced in 1 and 2 vol% GNT composite indicating that less overlapping had occurred between the GNP sheets as a result of the addition CNTs.

### Conclusions

Composites containing 1 vol% GNP displayed the highest saturation induction (2.39 T) and the lowest coercivity (583 A m<sup>-1</sup>), while the remanence values

**Table 1** Raman data of sintered materials

State	$R = I_D/I_G$	$\omega_G$ (cm <sup>-1</sup> )	$\omega_{2D}$ (cm <sup>-1</sup> )
Raw GNP	1.00	1573.0	2691.0
Raw CNT	1.11	1578.0	2691.0
0.5 vol% GNP composite	1.37	1581.6	2699.8
1 vol% GNP composite	1.15	1595.0	2708.6
2 vol% GNP composite	1.09	1595.8	2716.4
0.5 vol% GNT composite	1.07	1586.6	2710.7
1 vol% GNT composite	1.06	1583.2	2703.5
2 vol% GNT composite	1.06	1585.5	2709.0

were higher in the GNT composites than GNP composites for the same loading. The mechanical properties reveal a maximum increase in hardness of 18 % for the 1 vol% GNP composite. The highest tensile strength observed in the composite materials occurred in the 0.5 vol% GNT composite. The ordered nanocrystallite structure was promoted in the FeCo alloy by the addition of GNPs. Adding CNTs to the GNPs in FeCo leads to a more uniform and refined structure. However, porosity was induced leading to a decrease in the density of the GNT composites. Raman spectra show that the quality of the GNPs was improved by adding CNTs, which reduce the amount of overlapping of the GNP sheets.

## References

- [1] Kim H, Abdala AA, Macosko CW (2010) Graphene/polymer nanocomposites. *Macromolecules* 43:6515–6530. doi:[10.1021/ma100572e](https://doi.org/10.1021/ma100572e)
- [2] Tjong SC (2013) Recent progress in the development and properties of novel metal matrix nanocomposites reinforced with carbon nanotubes and graphene nanosheets. *Mater Sci Eng Rep* 74:281–350. doi:[10.1016/j.mser.2013.08.001](https://doi.org/10.1016/j.mser.2013.08.001)
- [3] Chen LY, Konishi H, Fehrenbacher A, Ma C, Xu JQ, Choi H, Xu HF, Pfefferkorn FE, Li XC (2012) Novel nanoprocessing route for bulk graphene nanoplatelets reinforced metal matrix nanocomposites. *Scr Mater* 67:29. doi:[10.1016/j.scriptamat.2012.03.013](https://doi.org/10.1016/j.scriptamat.2012.03.013)
- [4] Huang X, Qi X, Boey F, Zhang H (2012) Graphene-based composites. *Chem Soc Rev* 41:666–686. doi:[10.1039/c1cs15078b](https://doi.org/10.1039/c1cs15078b)
- [5] Wu ZS, Zhou GM, Yin LC, Ren W, Li F, Cheng HM (2012) Graphene/metal oxide composite electrode materials for energy storage. *Nano Energy* 1:107. doi:[10.1016/j.nanoen.2011.11.001](https://doi.org/10.1016/j.nanoen.2011.11.001)
- [6] Matsuda M, Yamashita K, Sago R, Akamine K, Takashima K, Nishida M (2012) Development of ductile B2-Type FeCo based alloys. *Mater Trans* 53:1826. doi:[10.2320/matertrans.M2012205](https://doi.org/10.2320/matertrans.M2012205)
- [7] Kawahara K, Uehara M (1984) A possibility for developing high strength soft magnetic materials in FeCo-X alloys. *J Mater Sci* 19:2575–2581. doi:[10.1007/Bf00550812](https://doi.org/10.1007/Bf00550812)
- [8] Kawahara K (1983) Effect of carbon on mechanical properties in Fe<sub>0.5</sub>Co<sub>0.5</sub> alloys. *J Mater Sci* 18:2047–2055. doi:[10.1007/BF00554997](https://doi.org/10.1007/BF00554997)
- [9] Yu RH, Ren L, Basu S, Unruh KM, Parvizi-Majidi A, Xiao JQ (2000) Novel soft magnetic composites fabricated by electrodeposition. *J Appl Phys* 87:5840–5842. doi:[10.1063/1.372540](https://doi.org/10.1063/1.372540)
- [10] Turgut Z, Huang M, Horwath JC, Fingers RT (2008) High strength bulk Fe–Co alloys produced by powder metallurgy. *J Appl Phys* 131–134:07E724. doi:[10.1063/1.2838466](https://doi.org/10.1063/1.2838466)
- [11] Rutz HG, Hanejko FG (1994) High density processing of high performance ferrous materials. In: International conference & exhibition on powder metallurgy & particulate material, Toronto
- [12] Xu CY, Jia SS, Cao ZY (2005) Synthesis of Al–Mn–Ce alloy by the spark plasma sintering. *Mater Charact* 54:394–398. doi:[10.1016/j.matchar.2004.12.006](https://doi.org/10.1016/j.matchar.2004.12.006)
- [13] Groza JR, Garcia M, Schneider JA (2001) Surface effects in field-assisted sintering. *J Mater Res* 16:286–292. doi:[10.1557/Jmr.2001.0043](https://doi.org/10.1557/Jmr.2001.0043)
- [14] Munir ZA, Anselmi-Tamburini U, Ohyanagi M (2006) The effect of electric field and pressure on the synthesis and consolidation of materials: a review of the spark plasma sintering method. *J Mater Sci* 41:763–777. doi:[10.1007/s10853-006-6555-2](https://doi.org/10.1007/s10853-006-6555-2)
- [15] Mani MK, Viola G, Reece MJ, Hall JP, Evans SL (2013) Structural and magnetic characterization of spark plasma sintered Fe-50Co alloys. In: MRS proceedings, vol 1516. Cambridge University Press, Cambridge, pp 201–207. doi:[10.1557/opl.2012](https://doi.org/10.1557/opl.2012)
- [16] Mani MK, Viola G, Reece MJ, Hall JP, Evans SL (2014) Improvement of interfacial bonding in carbon nanotube reinforced Fe–50Co composites by Ni–P coating: effect on magnetic and mechanical properties. *Mater Sci Eng B* 188:94–101. doi:[10.1016/j.mseb.2014.06.009](https://doi.org/10.1016/j.mseb.2014.06.009)
- [17] Mani MK, Viola G, Hall JP, Grasso S, Reece MJ (2015) Observation of Curie transition during spark plasma sintering of ferromagnetic materials. *J Magn Magn Mater* 382:202–205. doi:[10.1016/j.jmmm.2015.01.066](https://doi.org/10.1016/j.jmmm.2015.01.066)
- [18] Porwal H, Grasso S, Reece MJ (2014) Review of graphene–ceramic matrix composites. *Adv Appl Ceram* 112:443. doi:[10.1179/174367613x13764308970581](https://doi.org/10.1179/174367613x13764308970581)
- [19] Kim J, Cote LJ, Kim F, Yuan W, Shull KR, Huang J (2010) Graphene oxide sheets at interfaces. *J Am Chem Soc* 132:8180–8186. doi:[10.1021/ja102777p](https://doi.org/10.1021/ja102777p)
- [20] Wimalasiri Y, Zou LD (2013) Carbon nanotube/graphene composite for enhanced capacitive deionization performance. *Carbon* 59:464–471. doi:[10.1016/j.carbon.2013.03.040](https://doi.org/10.1016/j.carbon.2013.03.040)
- [21] Yazdani B, Porwal H, Xia YD, Yan HX, Reece MJ, Zhu YQ (2015) Role of synthesis method on microstructure and mechanical properties of graphene/carbon nanotube toughened Al<sub>2</sub>O<sub>3</sub> nanocomposites. *Ceram Int* 41:9813–9822. doi:[10.1016/j.ceramint.2015.04.054](https://doi.org/10.1016/j.ceramint.2015.04.054)

- [22] Yazdani B, Xia YD, Ahmad I, Zhu YQ (2015) Graphene and carbon nanotube (GNT)-reinforced alumina nanocomposites. *J Eur Ceram Soc* 35:179–186. doi:[10.1016/j.jeurceramsoc.2014.08.043](https://doi.org/10.1016/j.jeurceramsoc.2014.08.043)
- [23] Wang PN, Hsieh TH, Chiang CL, Shen MY (2015) Synergetic effects of mechanical properties on graphene nanoplatelet and multiwalled carbon nanotube hybrids reinforced epoxy/carbon fiber composites. *J Nanomater* 2015:1–9
- [24] Rashad M, Pan FS, Tang AT, Asif M, Aamir M (2014) Synergetic effect of graphene nanoplatelets (GNPs) and multi-walled carbon nanotube (MW-CNTs) on mechanical properties of pure magnesium. *J Alloy Compd* 603:111–118. doi:[10.1016/j.jallcom.2014.03.038](https://doi.org/10.1016/j.jallcom.2014.03.038)
- [25] Dieter GE (1986) *Mechanical metallurgy*, 3rd edn. McGraw-Hill, New York
- [26] Anderson P (2008) A universal DC characterisation system for hard and soft magnetic materials. *J Magn Magn Mater* 320:589–593. doi:[10.1016/j.jmmm.2008.04.034](https://doi.org/10.1016/j.jmmm.2008.04.034)
- [27] Mani MK, Viola G, Reece MJ, Hall JP, Evans SL (2014) Fabrication of carbon nanotube reinforced iron based magnetic alloy composites by spark plasma sintering. *J Alloy Compd* 601:146–153. doi:[10.1016/j.jallcom.2014.02.169](https://doi.org/10.1016/j.jallcom.2014.02.169)
- [28] Clegg DW, Buckley RA (1973) The disorder → order transformation in iron–cobalt-based alloys. *Met Sci* 7:48–54
- [29] Sahoo PK, Panigrahy B, Li D, Bahadur D (2013) Magnetic behavior of reduced graphene oxide/metal nanocomposites. *J Appl Phys* 113:17B525. doi:[10.1063/1.4799150](https://doi.org/10.1063/1.4799150)
- [30] Yuan BQ, Yu LM, Sheng LM, An K, Zhao XL (2012) Comparison of electromagnetic interference shielding properties between single-wall carbon nanotube and graphene sheet/polyaniline composites. *J Phys D Appl Phys* 45(23):1–6. doi:[10.1088/0022-3727/45/23/235108](https://doi.org/10.1088/0022-3727/45/23/235108)
- [31] Enoki T, Kobayashi Y (2005) Magnetic nanographite: an approach to molecular magnetism. *J Mater Chem* 15:3999–4002. doi:[10.1039/b500274p](https://doi.org/10.1039/b500274p)
- [32] Hug E, Hubert O, Guillot I (2000) Effect of strengthening on the magnetic behaviour of ordered intermetallic 2 % V-CoFe alloys. *J Magn Magn Mater* 215:197–200
- [33] Herzer G (1990) Grain size dependence of coercivity and permeability in nanocrystalline ferromagnets. *IEEE Trans Magn* 26:1397–1402
- [34] Wu HQ, Xu DM, Wang Q, Yao YZ, Wang QY, Su GQ (2008) Effect of heat treatment on structure and magnetic properties of FeCoNi/CNTs nanocomposites. *Bull Mater Sci* 31:801–806
- [35] Rao CN, Sood AK, Subrahmanyam KS, Govindaraj A (2009) Graphene: the new two-dimensional nanomaterial. *Angew Chem Int Ed Engl* 48(42):7752–7777. doi:[10.1002/anie.200901678](https://doi.org/10.1002/anie.200901678)
- [36] Bastwros M, Kim GY, Zhu C, Zhang K, Wang S, Tang X, Wang X (2014) Effect of ball milling on graphene reinforced Al6061 composite fabricated by semi-solid sintering. *Compos Part B Eng* 60:111–118. doi:[10.1016/j.compositesb.2013.12.043](https://doi.org/10.1016/j.compositesb.2013.12.043)
- [37] Ferrari AC, Meyer JC, Scardaci V, Casiraghi C, Lazzeri M, Mauri F, Piscanec S, Jiang D, Novoselov KS, Roth S, Geim AK (2006) Raman spectrum of graphene and graphene layers. *Phys Rev Lett* 97(1–4):187401. doi:[10.1103/PhysRevLett.97.187401](https://doi.org/10.1103/PhysRevLett.97.187401)
- [38] Inam F, Yan H, Reece MJ, Peijs T (2010) Structural and chemical stability of multiwall carbon nanotubes in sintered ceramic nanocomposite. *Adv Appl Ceram* 109(4):240–247